Contents lists available at AccScience Publishing
Nonlinear Science and Control Engineering (NSCE)
Vol. 1, No. 2 (2025)
https://accscience.com/journal/nsce

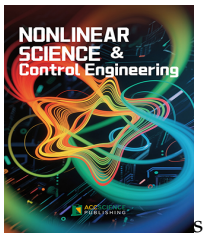

Magnetohydrodynamic mixed convective flow with thermal radiation and viscous dissipation: A homotopy perturbation approach

Babulal Talukdar[1] and Gopinath Mandal[2]*

[1]*Department of Mathematics, Saheed Nurul Islam Mahavidyalaya, Swarupnagar, West Bengal, India*
[2]*Department of Mathematics, Siksha Satra, A Central University of National Importance, Sriniketan, West Bengal, India*

Article History:
Received: August 6, 2025
Revised: September 12, 2025
Accepted: September 23, 2025
Published online: December 18, 2025

ABSTRACT

This study investigates the heat transfer characteristics of magnetohydrodynamic boundary-layer flow along a vertical surface, incorporating the effects of mixed convection, thermal radiation, viscous dissipation, and internal heat generation. The governing partial differential equations are transformed into dimensionless ordinary differential equations using appropriate dimensionless variables, and an analytical solution to these equations is obtained using the homotopy perturbation method. Various graphs illustrating velocity, temperature, skin friction, and heat transfer rate are presented and analyzed in detail. The findings reveal that increasing the radiation parameter reduces the skin friction coefficient by approximately 15.15% and the heat transfer rate by about 10%. The heat source parameter substantially increases the skin friction coefficient (by 72.84%) and the Nusselt number (by 87.80%). Furthermore, higher Eckert numbers raise the temperature profiles, whereas stronger magnetic fields and heat source parameters diminish the velocity profiles. The Prandtl number also plays a crucial role, with higher values resulting in a thinner thermal boundary layer. Consequently, the radiation parameter, heat generation, and Prandtl number are identified as key factors that enhance the model's performance. These results contribute to the development of advanced energy systems, industrial heat exchangers, and efficient cooling techniques.

Keywords: Heat generation; Homotopy perturbation method; Magnetic field; Mixed convection; Thermal radiation; Viscous dissipation

1. Introduction

The enhancement of heat transfer has garnered significant interest recently due to its wide range of industrial and engineering applications, including aerodynamics, power generation systems, liquid metal cooling, and thermal management in nuclear reactors. Soundalgekar et al.[1] examined the influence of free convection on Stokes flow over a vertical plate subjected to a transverse magnetic field, finding that the magnetic field suppresses velocity and alters heat transfer by damping fluid motion. Elbashbeshy[2] investigated magnetohydrodynamic (MHD) mass and heat

***Corresponding author**:
Gopinath Mandal (gopinath.mandal@visva-bharati.ac.in).

Citation:
Talukdar B, and Mandal G. Magnetohydrodynamic mixed convective flow with thermal radiation and viscous dissipation: A homotopy perturbation approach. *Nonlinear Sci Cont Eng*. 2025;1(2):025320009. doi: 10.36922/NSCE025320009

transfer over a vertical surface, incorporating the combined effects of thermal and concentration buoyancy. The study showed that buoyancy forces enhance velocity, while the magnetic field retards motion. Sivaiah et al.[3] explored the interaction of MHD and convective flow past a vertical permeable surface with thermal and mass transfer effects, demonstrating that permeability increases fluid velocity and improves heat transfer in porous media. Meanwhile, Zueco and Ahmed[4] investigated combined heat and mass transfer in an incompressible, viscous, electrically conducting fluid flowing over an infinite vertical porous plate under MHD conditions. They concluded that greater magnetic interaction reduces velocity but increases the thickness of the thermal boundary layer. Hamza[5] studied convection in an exothermic fluid flowing through a vertical channel, considering Newtonian heating and wall slip boundary conditions, and reported that wall slip reduces shear stress while Newtonian heating enhances temperature gradients near the wall.

In recent years, thermal radiation has become an important factor in heat transfer studies due to its relevance in advanced technologies such as space propulsion systems, gas-cooled nuclear reactors, rocket combustion chambers, and hypersonic flight vehicles. These developments emphasize the need to incorporate radiative heat transfer effects into flow and thermal analyses. Hossain and Takhar[6] examined the interaction of radiation with mixed convection flow over a vertical plate, reporting that radiation increases fluid temperature and thickens the thermal boundary layer. AboEldahab[7] analyzed radiative effects on heat transfer over a stretching surface in an electrically conducting fluid, finding that radiation elevates surface temperature but reduces heat transfer rates. Using the Laplace transform method, Muthucumaraswamy and Senthil[8] investigated heat and mass transfer over moving plates with thermal radiation effects and showed that radiation accelerates thermal response and reduces cooling time. Kho et al.[9] examined the combined influence of thermal radiation and magnetic fields on the boundary-layer flow of Casson nanofluids over a stretching sheet, concluding that radiation raises fluid temperature while magnetic fields suppress velocity. Kumar et al.[10] considered heat transfer from an infinite vertical plate with viscous dissipation, thermal radiation, and an external magnetic field, and found that viscous dissipation increases temperature within the boundary layer, intensifying thermal effects. Sattar and Kalim[11] studied unstable free convection in boundary layer flow over a vertical porous plate with thermal radiation, highlighting that radiation destabilizes the flow by enhancing thermal gradients. Cortell[12] explored the effects of radiation and viscous dissipation on thermal boundary layers over nonlinearly stretched sheets, concluding that both effects increase wall temperature and boundary layer thickness. Abel and Mahesha[13] analyzed heat transfer in MHD viscoelastic fluid flow over an extending sheet with variable thermal conductivity, a non-uniform heat source, and radiation, showing that variable conductivity enhances heat transfer while magnetic fields damp velocity. Kim[14] studied convective heat transfer with unstable MHD flow over a vertical porous extending surface with varying suction, demonstrating that suction stabilizes the flow and reduces thermal boundary layer thickness. Asogwa et al.[15] investigated hydromagnetic viscoelastic oscillatory flow in a porous medium with continuous suction and thermal radiation, showing that viscoelasticity has minimal influence on mass and heat transfer, and that suction and radiation dominate flow behavior. More recently, Pandey et al.[16] examined nonlinear radiation and buoyancy-driven mixed convection in Newtonian flow over a nonlinearly stretching vertical sheet, reporting that nonlinear radiation significantly increases fluid temperature. Mandal[17] analyzed convection and radiation effects in micropolar nanofluid flow over a vertically nonlinear stretching sheet, finding that radiation enhances microrotation and thermal boundary layer thickness.

Viscous dissipation has also attracted considerable attention due to its significance in various industrial processes, such as glass fiber manufacturing, cooling systems, material handling, and drying processes in the textile and paper industries, as well as plastic sheet extrusion in aerodynamic applications. Viscous dissipation significantly influences heat transfer rates and local temperature variations, especially in low-temperature fluid flow environments, making it an essential factor when optimizing thermal systems. Israel-Cookey et al.[18] analyzed the effects of viscous dissipation and thermal radiation on unsteady free convective MHD flow over a stretchable heated vertical plate embedded in a porous medium with time-dependent suction, demonstrating that viscous dissipation increases wall temperature while suction stabilizes the boundary layer. Pal et al.[19] examined the combined effects of Ohmic and viscous dissipation on mixed convection, thermal radiation, and MHD heat and mass transfer over a stretching sheet, showing that viscous dissipation greatly intensifies thermal energy storage in copper–water nanofluids. Abel et al.[20] investigated hydromagnetic viscoelastic flow with Ohmic and viscous dissipation over an extending surface, concluding that Joule heating raises fluid temperature while magnetic fields oppose fluid motion. Sharma et al.[21] studied the influence of an external magnetic field on unsteady micropolar fluid flow and heat transfer with viscous dissipation, confirming that magnetic damping decreases velocity while dissipation increases temperature. Mandal[22] further examined magnetic field effects on radiative tri-hybrid nanofluid flow over a shrinking surface, focusing on entropy generation, and showed that entropy production increases with stronger magnetic and radiation effects. Due to the inherently nonlinear nature of most MHD-related problems, exact analytical solutions are uncommon, and alternative solution methods are often required. Semi-analytical techniques combined with numerical approaches have been shown to yield valuable results. Since He's pioneering work on the homotopy perturbation method (HPM),[23–25] numerous researchers, including Beléndez et al.[26] and Ganji and Ganji,[27] have adopted HPM to solve nonlinear differential equations, demonstrating its rapid convergence and reliable approximations for complex flow problems.

For example, Ganji and Ganji[27] applied HPM to the thermal boundary layer problem over a semi-infinite flat plate and obtained analytical solutions expressed as rapidly converging infinite series. Their results demonstrated that HPM serves as an effective alternative to numerical methods. Jhankal[28] used He's HPM to solve two-dimensional steady free convection of water at 40°C through a highly porous medium bounded by a moving vertical plate under a transverse magnetic field, showing that magnetic fields damp velocity while porous media enhance convective heat transfer.

1.1. Research gaps and novel contributions

While the HPM has been successfully applied to MHD boundary-layer problems in prior studies, most of these investigations were restricted to simplified cases that either neglected thermal radiation or internal heat generation or treated them separately. The novelty of the present work lies in:

(i) Simultaneous incorporation of radiation and heat generation within the HPM framework. Earlier HPM-based studies generally considered radiation alone (e.g., Cortell[12]) or viscous dissipation without radiation/heat generation (e.g., Abel et al.[20]). In contrast, this study integrates both Rosseland-type thermal radiation and a volumetric heat source parameter into the governing energy equation, thereby capturing their coupled influence on boundary-layer dynamics.

(ii) Extension of HPM to a more complex parameter space. By embedding radiation and heat-generation terms directly into the homotopy formulation, the present work expands HPM beyond the scope of conventional nonlinear conduction–convection problems. This results in closed-form analytical approximations that remain valid even when heat generation and radiation effects are significant—a scenario rarely addressed in existing literature.

(iii) Quantitative comparison showing their impact. The study provides explicit numerical evidence for the skin-friction and Nusselt number. Such combined insights have not been reported in earlier HPM-based analyses, which typically focused on single-effect variations.

2. Formulation of the problem

Consider a viscous, dissipative fluid flowing steadily through a porous medium under mixed convection and thermal radiation, bounded by a vertical plate that slides with a constant velocity U_0 while subjected to a uniform normal suction. The coordinate system is chosen such that the x*-axis lies along the plate and the y*-axis is perpendicular to it. A uniform and strong transverse magnetic field H_0 is applied to the plate, with all fluid properties assumed constant (see Figure 1). The Reynolds number for the flow is sufficiently low that induced magnetic field effects may be neglected. Under the classical boundary-layer approximations, the governing equations are formulated accordingly.

The fluid is assumed to be in thermal equilibrium, and owing to the small magnetic Reynolds number, both electric-field and induced-magnetic-field effects are considered negligible. The mathematical model incorporates a unique porous medium and accounts for the combined influences of viscous dissipation and mixed convection, as described by Pal et al.[29]

Continuity equation:

$$\frac{\partial v^*}{\partial y^*} = 0 \tag{1}$$

Momentum equation:

$$v^* \frac{\partial u^*}{\partial y^*} = g\beta \left(T^* - T^*_\infty\right)^2 + \nu \frac{\partial^2 u^*}{\partial y^{*2}} - \frac{\nu}{K^*} u^* - \frac{\sigma H_0^2}{\rho} u^* \tag{2}$$

Energy equation:

$$\begin{aligned} v^* \frac{\partial T^*}{\partial y^*} = \frac{\kappa}{\rho C_p} \frac{\partial^2 T^*}{\partial y^{*2}} + \frac{\nu}{C_p} \left(\frac{\partial u^*}{\partial y^*}\right)^2 \\ - \frac{1}{\rho C_p} \frac{\partial q_r}{\partial y^*} - \frac{Q^*}{\rho C_p} \left(T^* - T^*_\infty\right) \end{aligned} \tag{3}$$

where $q_r = \frac{-4\sigma^* \partial T^{*4}}{3k^* \partial y^*}$ and $T^{*4} \approx 4T^{*3}_\infty T^* - 3T^{*4}_\infty$ (Pal and Mandal[30]).

The corresponding boundary conditions are:

$$u^* = U_0,\ T^* = T^*_w, \quad at\ y^* = 0$$

$$u^* \to 0,\ T^* \to T^*_\infty, \quad for\ y^* \to \infty \tag{4}$$

From Equation (1), we obtain $v^* = -v_0$, a constant suction.

Using the following non-dimensional parameters in Equations (2) and (3):

$$y = \frac{U_0 y^*}{\nu},\ u = \frac{u^*}{U_0},\ \theta = \frac{T^* - T^*_\infty}{T^*_w - T^*_\infty}, K = \frac{K^* U_0^2}{\nu^2},$$

$$\lambda = \frac{v_0}{U_0}, G_r = \frac{\nu g\beta \left(T^* - T^*_\infty\right)^2}{U_0^3},$$

$$M = \frac{\sigma H_0^2 \nu}{\rho U_0^2},\ P_r = \frac{\mu C_p}{\kappa},$$

$$\mu = \rho\nu, \quad E_c = \frac{U_0^2}{C_p \left(T^* - T^*_\infty\right)},$$

$$R_d = \frac{16\sigma^* T^{*3}_\infty}{3k^*\kappa},\ R = \frac{Q^*\nu}{\rho C_p U_0^2}$$

we get,

$$\frac{\partial^2 u}{\partial y^2} + \lambda \frac{\partial u}{\partial y} - \left(M + \frac{1}{K}\right) u + G_r \theta^2 = 0 \tag{5}$$

$$\left(1 + R_d\right) \frac{\partial^2 \theta}{\partial y^2} + P_r \lambda \frac{\partial \theta}{\partial y} - P_r R \theta + P_r E_c \left(\frac{\partial u}{\partial y}\right)^2 = 0. \tag{6}$$

The associated boundary conditions become:

$$\begin{aligned} u = 1, \theta = 1, at y = 0, \\ u \to 0, \theta \to 0,\ for\ y \to \infty \end{aligned} \tag{7}$$

where the suction parameter, permeability parameter, Hartmann number, Grashof number, Eckert number, Prandtl number, radiation parameter, and heat-source parameter are denoted by λ, K, M, G_r, E_c, P_r, R_d, and R.

3. Method of solution

The HPM is a semi-analytical approach designed to solve both linear and nonlinear differential equations. Over the past two decades, HPM has been widely utilized to address numerous nonlinear ordinary and partial differential equations across various fields such as science, finance, and engineering. The method constructs a homotopy—a continuous transformation—connecting a simpler problem with a known solution to the original complex equation. An embedding parameter, often denoted as (p) or (q), varying from 0 to 1, serves as an artificial small parameter to facilitate the perturbation process. Unlike classical perturbation techniques, HPM does not require an inherent small parameter in the governing equations, allowing it to generate approximations valid even for large parameter values. The solution is expressed as a series expansion in terms of the embedding parameter, which successively refines the approximate solution. One notable

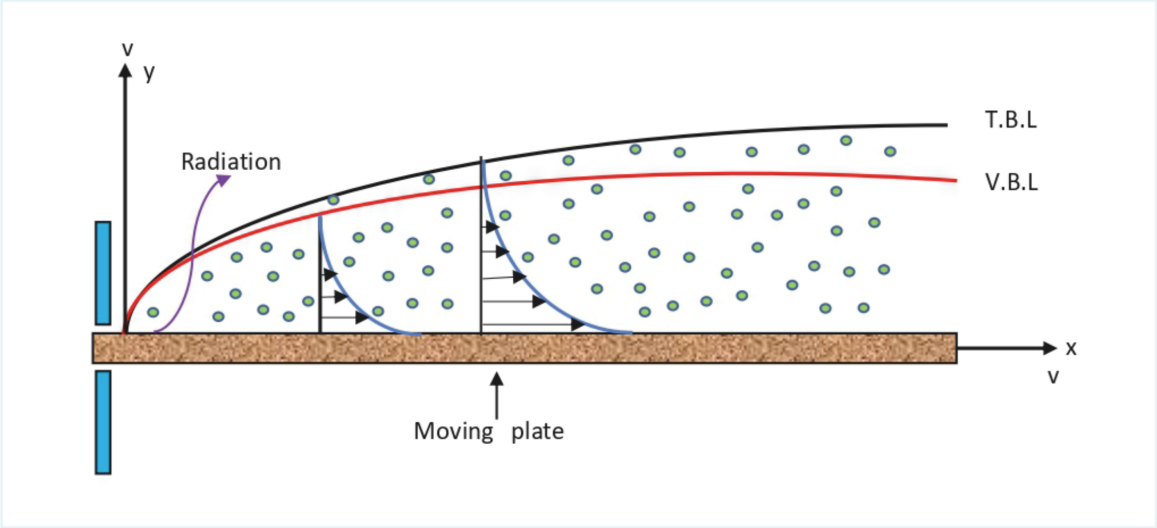

Figure 1. Flow configuration
Abbreviations: T.B.L.: Thermal boundary layer; V.B.L.: Velocity boundary layer.

advantage of HPM is its ability to provide uniformly valid approximations and to demonstrate natural convergence of the solution series, a feature not commonly seen in many analytical or semi-analytical methods for nonlinear partial differential equations. To illustrate the fundamental concept of HPM, we consider a nonlinear differential equation as formulated by He.[23,24]

$$C(u) - f(r) = 0, \quad r \in \mho \tag{8}$$

depending on the condition at the boundary

$$D\left(u, \frac{\partial u}{\partial y}\right) = 0, r \in \Im, \tag{9}$$

where C and D denote a boundary operator and a generic differential operator, respectively. f (r) is a known analytic function, u (x,t) is an unknown function, $\Im$ is the domain border of $\mho$, and $\frac{\partial}{\partial y}$ represents severaliation along the outward normal vector from $\mho$.

The severalial operator C may be separated into two components, L (linear) and N (nonlinear). Consequently, we rewrite Equation (8) as follows:

$$L(u) + N(u) - f(r) = 0 \tag{10}$$

Introducing a synthetic parameter q into Equation (10) in the following manner:

$$L(u) + q\left(N(u) - f(r)\right) = 0, \tag{11}$$

where q in [0,1].

We create a homotopy of the form, using HPM:

v(r,q): $\mho \times [0,1] \to R$ to Equation (4) that satisfies:

$$H(v,q) = (1-q)\left[L(v) - L\left(u_0\right)\right] + q\left[L(v) + N(v) - f(r) = 0,\right.$$

i.e.,

$$H(v,q) = L(v) - L\left(u_0\right) + qL\left(u_0\right) + q\left[N(v) - f(r)\right] = 0, \tag{12}$$

where $u_0(x,t)$ is the initial approximation that satisfies the boundary condition of Equation (9). Evidently, these definitions yield:

$$H(v,0) = L(v) - L\left(u_0\right) = 0$$

$$and\ H(v,1) = C(v) - f(r) = 0$$

The transformation of q from zero to unity is equivalent to the transformation of $v(r,q)$ from u_0 (r) to $u(r)$. Topology refers to this process as deformation, whereas $L(v)$–$L(u_0)$ and $C(v) - f(r)$ are referred to as the homotopy.

We assume that the solution to Equation (12) may be expressed as a power series in q, given that q in [0,1] is treated as a small parameter:

$$v = v_0 + qv_1 + q^2 v_2 + \cdots \ldots \tag{13}$$

By choosing q = 1, the approximate solution of Equation (8) is obtained.

$$u(x,t) = \lim_{q \to 0} v_n = v_0 + v_1 + v_2 + \cdots \ldots \tag{14}$$

The convergence and stability of this method were demonstrated by Nia et al.[31]

4. Solution using the homotopy perturbation method

According to HPM, the homotopy form of Equations (5) and (6) is constructed as follows:

$$(1-q)\left[\frac{\partial^2 u}{\partial y^2} + \lambda\frac{\partial u}{\partial y} - \left(M + \frac{1}{K}\right)u\right] + q\left[\frac{\partial^2 u}{\partial y^2} + \lambda\frac{\partial u}{\partial y} - \left(M + \frac{1}{K}\right)u + G_r\theta^2\right] = 0 \tag{15}$$

$$(1-q)\left[(1+R_d)\frac{\partial^2 \theta}{\partial y^2} + P_r\lambda\frac{\partial \theta}{\partial y} - P_r R\theta\right] + q\left[(1+R_d)\frac{\partial^2 \theta}{\partial y^2} + P_r\lambda\frac{\partial \theta}{\partial y} - P_r R\theta + P_r E_c\left(\frac{\partial u}{\partial y}\right)^2\right] = 0. \tag{16}$$

We consider u and θ as the following:

$$u = u_0 + qu_1 + q^2 u_1 \cdots \ldots \tag{17}$$

$$\theta = \theta_0 + q\theta_1 + q^2\theta_1 \cdots \ldots \tag{18}$$

Substituting Equations (17)) and (18) into Equations (15) and (16), equating like terms, and neglecting higher orders of q, we obtain:

$$\frac{\partial^2 u_0}{\partial y^2} + \lambda \frac{\partial u_0}{\partial y} - \left(M + \frac{1}{K}\right) u_0 = 0, \tag{19}$$

$$\frac{\partial^2 u_1}{\partial y^2} + \lambda \frac{\partial u_1}{\partial y} - \left(M + \frac{1}{K}\right) u_1 + G_r \theta_0^2 = 0, \tag{20}$$

$$(1 + R_d) \frac{\partial^2 \theta_0}{\partial y^2} + P_r \lambda \frac{\partial \theta_0}{\partial y} - P_r R \theta_0 = 0, \tag{21}$$

$$(1 + R_d) \frac{\partial^2 \theta_1}{\partial y^2} + P_r \lambda \frac{\partial \theta_1}{\partial y} - P_r R \theta_1 + P_r E_c \left(\frac{\partial u_0}{\partial y}\right)^2 = 0, \tag{22}$$

The corresponding boundary conditions are:

$$u_0 = 1,\ u_1 = 0,\ \theta_0 = 1,\ \theta_1 = 0 \quad \text{at } y = 0,$$

$$u_0 \to 0,\ u_1 \to 0,\ \theta_0 \to 0,\ \theta_1 \to 0 \quad \text{as } y \to \infty. \tag{23}$$

Solving Equations (19)–(22) with boundary conditions Equation (23), we obtain:

$$u_0 = d_1 e^{a_1 y} + d_2 e^{a_2 y} \tag{24}$$

$$\theta_0 = d_3 e^{a_3 y} + d_4 e^{a_4 y} \tag{25}$$

$$u_1 = d_5 e^{a_1 y} + d_6 e^{a_2 y} + d_7 e^{2a_3 y} + d_8 e^{2a_4 y} + d_9 e^{(a_3 + a_4) y} \tag{26}$$

$$\theta_1 = d_{12} e^{a_3 y} + d_{13} e^{a_4 y} + d_{14} e^{2a_1 y} + d_{15} e^{2a_2 y} + d_{16} e^{(a_1 + a_2) y}. \tag{27}$$

The constant coefficients can be calculated using the boundary condition $y = \infty$, which is replaced by y = 10 in accordance with standard practice in boundary-layer analysis. If $q \longrightarrow 1$, we obtain the approximate solutions of Equations (15) and (16). The constant coefficients $a_i (i = 1, 2, 3, 4)$ and $d_j (j = 1, 2, \ldots..18)$ are defined as in the **Appendix**.

5. Physical quantities

5.1. Skin friction

Skin friction refers to the resistive force experienced by a body moving through a fluid due to the frictional interaction between the fluid and the surface of the object. This phenomenon is a form of drag, commonly called viscous drag or surface friction drag, and is a critical factor in fluid dynamics. The origin of skin friction lies in the fluid's viscosity, which produces shear stress at the interface between the fluid and the object's surface. The viscous shear stress acting on the surface of the plate can be expressed as:

$$C_{f_x} = -\left(\frac{\partial u}{\partial y}\right)_{y=0} \tag{28}$$

5.2. Rate of heat transfer

The Nusselt number (Nu) is a dimensionless parameter used in convective heat transfer to measure the ratio of convective to conductive heat transfer. It serves as an indicator of heat-transfer efficiency in a fluid-flow system; a larger Nusselt number corresponds to enhanced convective heat transfer. The dimensionless expression for the heat-transfer rate at the plate surface, commonly known as the Nusselt number, is given by:

$$Nu_x = -\left(\frac{\partial \theta}{\partial y}\right)_{y=0} \tag{29}$$

6. Results and discussions

Equations (15) and (16) were solved under steady-state conditions with boundary condition (Equation (18)) using HPM, which is recognized as one of the most effective analytical solution techniques. We also numerically solved the equations using MATLAB solver bvp4c and compared the results with those obtained from HPM. The bvp4c solver is based on the collocation method with the Lobatto IIIa formula, which provides reliable solutions for highly nonlinear ordinary differential equations arising from similarity transformations.

The influence of various parameters on velocity and temperature is illustrated through graphical analysis. Table 1 compares the computed Nusselt number Nu_x for $R = 0.0, \lambda = 0.0, R_d = 0.0, M = 0.0, G_r = 0.0, K = 0.0$, and $E_c = 0$ across different Prandtl numbers P_r, showing excellent agreement with previously reported results by Wang[32] and Hussain et al.[33] Additional numerical data in Tables 2–4 highlight how parameter variations affect heat-transfer rates and skin-friction coefficients. These results also show that HPM, being an analytical method, provides accurate results consistent with those computed using the bvp4c technique.

Hence, HPM offers significant advantages over purely numerical techniques such as bvp4c, as it provides approximate analytical solutions without requiring discretization, linearization, or the presence of small parameters. The method is simple, computationally efficient, and exhibits rapid convergence, with only a few terms in the series solution needed to achieve high accuracy, as demonstrated by the close agreement with benchmark and numerical results in Tables 1–5. Unlike black-box numerical solvers, HPM preserves the analytical structure of the solution, offering clearer insight into the effects of governing parameters on flow and heat-transfer behavior. This dual benefit of accuracy and analytical interpretability makes HPM a powerful and versatile tool for solving complex nonlinear problems in fluid dynamics and heat transfer.

The Prandtl number P_r is a crucial dimensionless parameter in fluid mechanics and heat transfer that characterizes fluid properties by comparing momentum diffusivity (kinematic viscosity) to thermal diffusivity. Named after Ludwig Prandtl, this parameter indicates the relative thickness of the velocity and thermal boundary layers. Fluids with low P_r exhibit high thermal conductivity and are ideal for efficient heat transfer. As shown in Figure 2, an increase in P_r results in reduced velocity, indicating that thermal diffusivity governs the thinning of the thermal boundary layer. Figure 3 further illustrates hat fluid temperature decreases with increased thermal diffusivity, consistent with boundary conditions. Higher P_r values impede fluid-particle movement at elevated temperatures, thereby reducing thermal conductivity within the flow. Thus, physically, a higher P_r corresponds to sluggish heat transport and

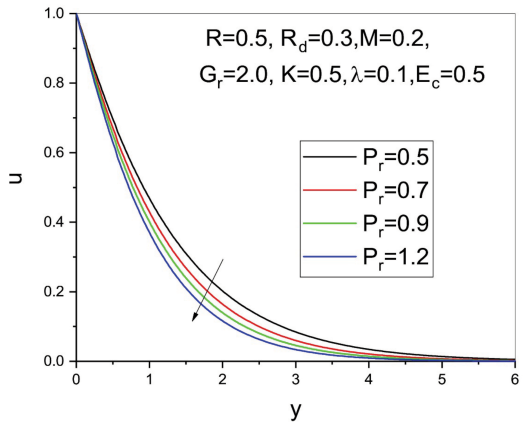

Figure 2. Velocity profiles for Prandtl number P_r
Abbreviations: E_c: Eckert number; G_r: Grashof number; K: Permeability parameter; M, Hartmann number; R: Heat-source parameter; R_d: Radiation parameter; λ: Suction parameter.

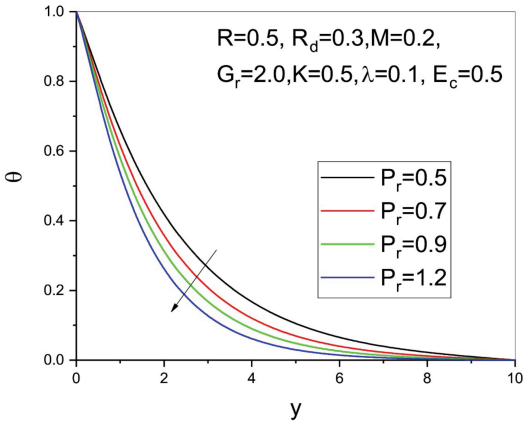

Figure 3. Temperature profiles for Prandtl number P_r
Abbreviations: E_c: Eckert number; G_r: Grashof number; K: Permeability parameter; M: Hartmann number; R: Heat-source parameter; R_d: Radiation parameter; λ: Suction parameter.

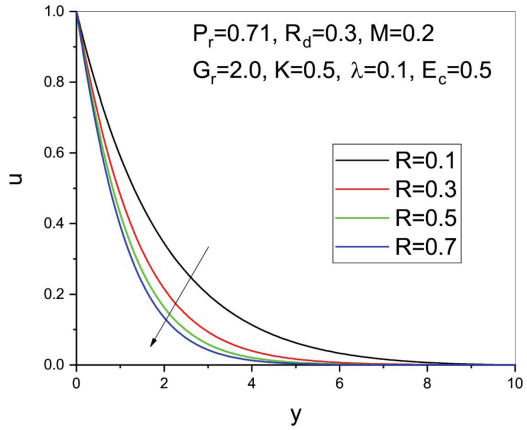

Figure 4. Velocity profiles for heat-source parameter R
Abbreviations: E_c: Eckert number; G_r: Grashof number; K: Permeability parameter; M: Hartmann number; P_r: Prandtl number; R_d: Radiation parameter; λ: Suction parameter.

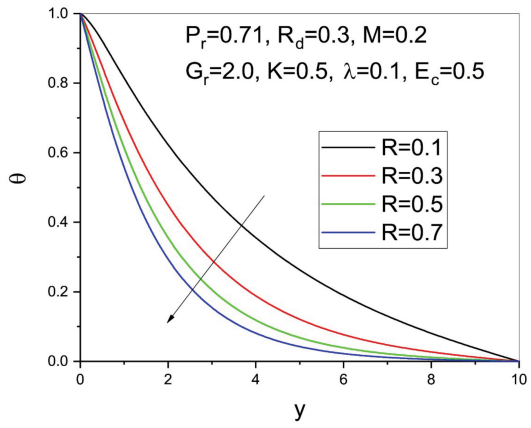

Figure 5. Temperature profiles for heat-source parameter R
Abbreviations: E_c: Eckert number; G_r: Grashof number; K: Permeability parameter; M: Hartmann number; P_r: Prandtl number; R_d: radiation parameter; λ: Suction parameter.

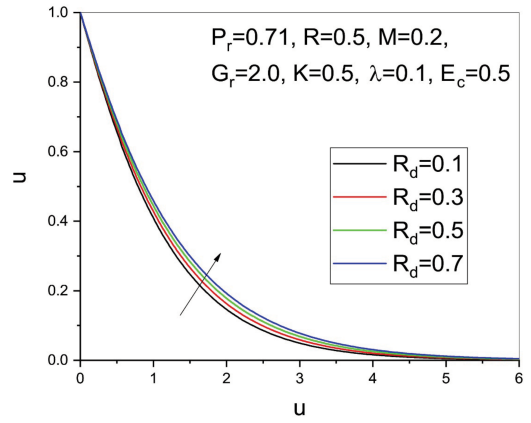

Figure 6. Velocity profiles for the radiation parameter R_d
Abbreviations: E_c: Eckert number; G_r: Grashof number; K: Permeability parameter; M: Hartmann number; P_r: Prandtl number; R: Heat-source parameter; λ: Suction parameter.

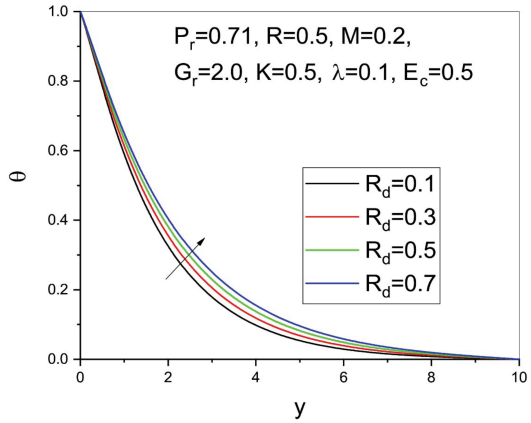

Figure 7. Temperature profiles for the radiation parameter R_d
Abbreviations: E_c: Eckert number; G_r: Grashof number; K: Permeability parameter; M: Hartmann number; P_r: Prandtl number; R: Heat-source parameter; λ: Suction parameter.

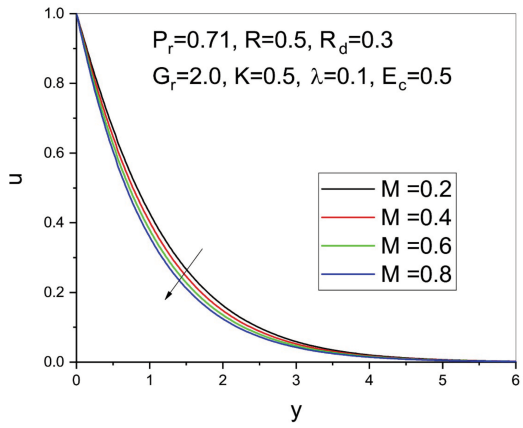

Figure 8. Velocity profiles for magnetic-field parameter M
Abbreviations: E_c: Eckert number; G_r: Grashof number; K: Permeability parameter; P_r: Prandtl number; R: Heat-source parameter; R_d: Radiation parameter; λ: Suction parameter.

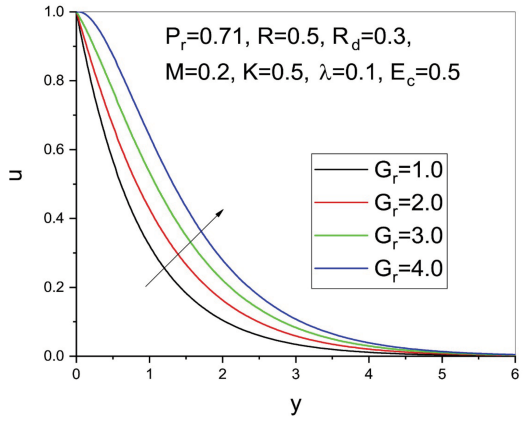

Figure 9. Velocity profiles for thermal Grashof number G_r
Abbreviations: E_c: Eckert number; K: Permeability parameter; M: Hartmann number; P_r: Prandtl number; R: Heat-source parameter; R_d: Radiation parameter; λ: Suction parameter.

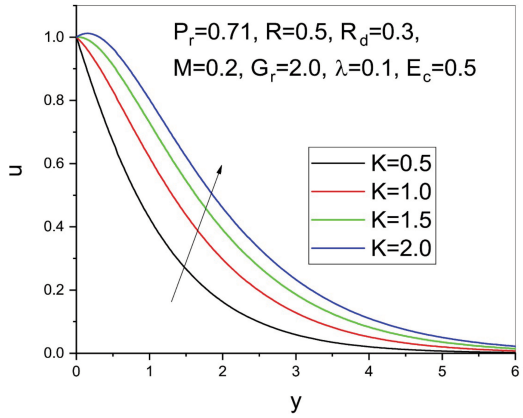

Figure 10. Velocity profiles for permeability parameter K
Abbreviations: E_c: Eckert number; G_r: Grashof number; M: Hartmann number; P_r: Prandtl number; R: Heat-source parameter; R_d: Radiation parameter; λ: Suction parameter.

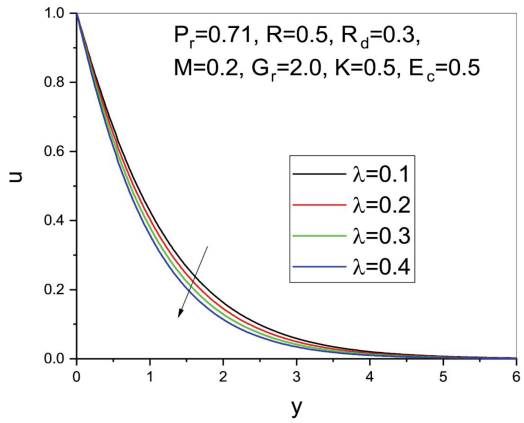

Figure 11. Velocity profiles for the suction parameter λ
Abbreviations: E_c: Eckert number; G_r: Grashof number; K: Permeability parameter; M: Hartmann number; P_r: Prandtl number; R: Heat-source parameter; R_d: Radiation parameter.

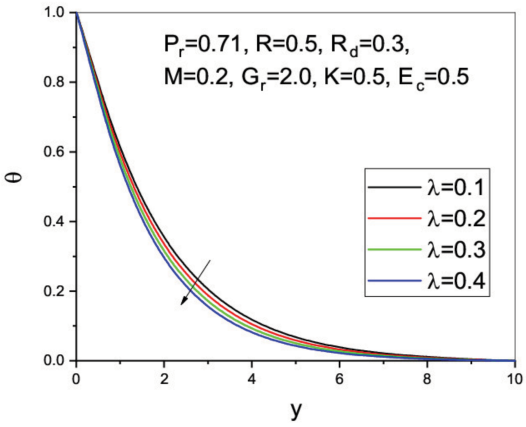

Figure 12. Temperature profiles for the suction parameter λ
Abbreviations: E_c: Eckert number; G_r: Grashof number; K: Permeability parameter; M: Hartmann number; P_r: Prandtl number; R: Heat-source parameter; R_d: Radiation parameter.

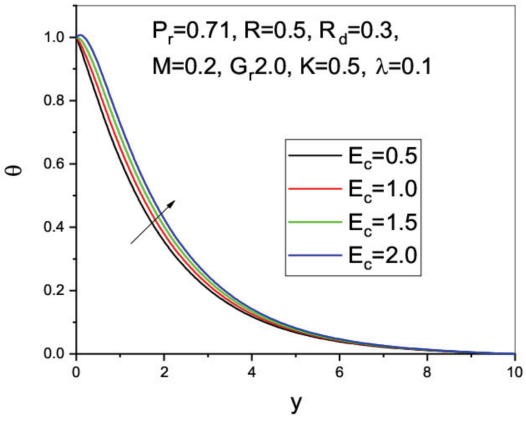

Figure 13. Temperature profiles for the Eckert number E_c
Abbreviations: G_r: Grashof number; K: Permeability parameter; M: Hartmann number; P_r: Prandtl number; R: Heat-source parameter; R_d: Radiation parameter; λ: Suction parameter.

Table 1. Comparison of results for Nusselt number Nu_x when $R = 0.0$, R_d= 0.0, $M = 0.0$, G_r= 0.0, $K = 0.0$, $\lambda = 0.0$, and E_c= 0.0

$\mathbf{P_r}$	Wang[32]	Hussain et al.[33]	Our results using HPM	Our results using bvp4c
0.7	0.4539	0.4582	0.4582	0.4570
2.0	0.9114	0.9114	0.9113	0.9112
7.0	1.8954	1.8954	1.8954	1.8961
20	3.3539	3.3539	3.3539	3.3548
70	6.4622	6.4622	6.4621	6.4605

Abbreviations: E_c: Eckert number; G_r: Grashof number; HPM: Homotopy perturbation method; K: Permeability parameter; M: Hartmann number; P_r: Prandtl number; R: Heat-source parameter; R_d: Radiation parameter; λ: Suction parameter.

Table 2. Effects of P_r on C_{f_x} and Nusselt number Nu_x with $R = 0.5$, R_d= 0.3, $M = 0.2$, G_r= 2.0, $K = 0.5$, $\lambda = 0.1$, and E_c= 0

	Our results by HPM		Our results by bvp4c	
P_r	C_{fx}	Nu_x	C_{fx}	Nu_x
0.5	0.683336	0.328566	0.6821	0.3274
0.7	0.742687	0.368590	0.7440	0.3702
0.9	0.788391	0.399133	0.7869	0.3981
1.2	0.841624	0.433757	0.8430	0.4352

Abbreviations: C_{f_x}: Skin friction coefficient; E_c: Eckert number; G_r: Grashof number; HPM: Homotopy perturbation method; K: Permeability parameter; M: Hartmann number; P_r: Prandtl number; R: Heat-source parameter; R_d: Radiation parameter; λ: Suction parameter.

Table 3. Effects of R on C_{f_x} and Nusselt number Nu_x with P_r= 0.71, R_d= 0.3, $M = 0.2$, G_r= 2.0, $K = 0.5$, $\lambda = 0.1$, and E_c= 0.5

	Our results by HPM		Our results by bvp4c	
P_r	C_{fx}	Nu_x	C_{fx}	Nu_x
0.1	0.519161	0.071028	0.5187	0.0705
0.3	0.664837	0.246802	0.6634	0.2471
0.5	0.745240	0.370307	0.7445	0.3709
0.7	0.800553	0.470625	0.8012	0.4712

Abbreviations: C_{f_x}: Skin friction coefficient; E_c: Eckert number; G_r: Grashof number; HPM: Homotopy perturbation method; K: Permeability parameter; M: Hartmann number; P_r: Prandtl number; R: Heat-source parameter; R_d: Radiation parameter; λ: Suction parameter.

Table 4. Effects of R_d on C_{f_x} and Nusselt number Nu_x with $P_r = 0.71$, $R = 0.5$, $M = 0.2$, $G_r = 2.0$, $K = 0.5$, $\lambda = 0.1$, and $E_c = 0.5$

	Our results by HPM		Our results by bvp4c	
P_r	C_{fx}	Nu_x	C_{fx}	Nu_x
0.1	0.775555	0.390606	0.7761	0.3910
0.3	0.745240	0.370307	0.7449	0.3706
0.5	0.719659	0.353074	0.7202	0.3529
0.7	0.697633	0.338210	0.6981	0.3385

Abbreviations: C_{f_x}: Skin friction coefficient; E_c: Eckert number; G_r: Grashof number; HPM: Homotopy perturbation method; K: Permeability parameter; M: Hartmann number; P_r: Prandtl number; R: Heat-source parameter; R_d: Radiation parameter; λ: Suction parameter.

Table 5. Effects of λ on C_{f_x} and Nusselt number Nu_x with P_r= 0.71, $R = 0.5$, R_d= 0.3, $M = 0.2$, G_r= 2.0, E_c= 0.5, and $K = 0.5$

	Our results by HPM		Our results by bvp4c	
P_r	C_{fx}	Nu_x	C_{fx}	Nu_x
0.1	0.745240	0.370307	0.7447	0.3700
0.2	0.801296	0.391416	0.8005	0.3919
0.3	0.860361	0.413729	0.8611	0.4142
0.4	0.922349	0.437224	0.9215	0.4377

Abbreviations: C_{f_x}: Skin friction coefficient; E_c: Eckert number; G_r: Grashof number; HPM: Homotopy perturbation method; K: Permeability parameter; M: Hartmann number; P_r: Prandtl number; R: Heat-source parameter; R_d: Radiation parameter; λ: Suction parameter.

restricted fluid motion, whereas a lower P_r enhances thermal diffusion and promotes effective heat transfer.

The heat-source parameter R quantifies internal heat generation within the fluid system, affecting temperature and velocity profiles. Figures 4 and 5 depict a decrease in both velocity and temperature as R increases, suggesting that internal heat sources can retard fluid motion and thermal diffusion.

The thermal radiation parameter R_d quantifies the impact of radiative heat transfer on the overall heat exchange process. Figure 6 shows that increasing R_d accelerates fluid velocity, indicating that radiation enhances flow dynamics. Correspondingly, Figure 7

reveals that higher R_d increases fluid temperature and thickens the thermal boundary layer due to augmented radiative energy absorption. This enhanced radiative exchange leads to more pronounced temperature gradients at the surface. Essentially, thermal radiation supplements molecular conduction with external heat energy, thereby elevating the temperature profile.

In the context of MHD flow, Figure 8 demonstrates that increasing the magnetic parameter M reduces fluid velocity due to the Lorentz force acting as a drag opposing motion. Physically, stronger transverse magnetic fields suppress fluid motion, leading to momentum damping. This suppression modifies the balance between convection and conduction, offering a means to control heat-transfer characteristics in electrically conducting fluids.

The thermal Grashof number G_r measures the ratio of buoyancy to viscous forces. Figure 9 illustrates that as G_r increases, the velocity profile is enhanced due to dominant buoyant forces, strengthening natural convection. The parameter G_r thus represents the relative influence of thermal buoyancy compared to viscous forces within the boundary layer.

Figure 10 shows velocity profiles as a function of distance from the wall for different permeability parameters K. Physically, higher permeability corresponds to a more porous medium that offers less resistance to flow, allowing fluid to pass through more freely. An increase in permeability reduces flow resistance, leading to higher velocities. Suction, represented by the parameter λ, is commonly used in MHD flow control. It influences velocity such that $\lambda > 0$ indicates suction, $\lambda < 0$ denotes injection, and $\lambda = 0$ corresponds to no suction/injection. Figure 11 reveals that increased suction lowers the velocity profile by withdrawing fluid momentum from the surface. Likewise, Figure 12 shows that suction reduces temperature profiles by removing heat, thereby thinning the thermal boundary layer.

The Eckert number E_c relates kinetic energy dissipation to thermal-energy generation. Figure 13 indicates that increasing E_c raises fluid temperature as viscous dissipation converts kinetic energy into heat, thickening the thermal boundary layer and affecting heat-transfer efficiency.

Tables 2–4 present numerical results for the heat-transfer coefficient Nu_x and skin-friction coefficient C_{f_x}. It is evident that increasing the Prandtl number P_r, the heat-source parameter R, and the suction parameter λ enhances both C_{f_x} and Nu_x, while a higher thermal-radiation parameter R_d reduces these values. Table 3 shows that increasing R_d decreases skin friction by 15.15% and the heat-transfer rate by 10%. Conversely, Table 4 indicates a 72.84% rise in skin friction and an 87.80% increase in the Nusselt number due to a higher heat-source parameter R. Suction also significantly enhances skin friction by 56.10% and the Nusselt number by 21.11%.

7. Applications

The present study has several practical implications in engineering and applied sciences, where the combined effects of magnetic fields, thermal radiation, viscous dissipation, and internal heat generation significantly influence fluid flow and heat-transfer phenomena. Key application areas include:

(i) Energy and power systems
Cooling of nuclear reactors, gas turbines, and solar collectors, where radiative heat transfer and viscous dissipation play critical roles.

(ii) Aerospace and space technology
Thermal protection in re-entry vehicles, spacecraft, and missiles, where strong radiative and viscous effects occur under extreme conditions.

(iii) Manufacturing and industrial processes
Polymer extrusion, continuous casting, and metal processing, where control of thermal boundary layers is essential; glass fiber manufacturing; drying operations in the textile and paper industries; and plastic-sheet production involving dissipative heating.

(iv) Electronics cooling and advanced devices
Micro-electro-mechanical systems and semiconductor cooling using MHD-based nanofluid techniques; compact heat exchangers with enhanced thermal performance.

(v) Environmental and biomedical systems
Thermal regulation in filtration processes, flue-gas treatment, and nuclear-waste management; modeling of biofluids (blood analogues) under magnetic fields for medical imaging and targeted therapies.

These applications highlight the importance of integrating MHD effects, radiation, and dissipation into modern designs, contributing to efficient thermal management, enhanced safety, and sustainable engineering solutions.

8. Conclusion

The effects of MHD flow and thermal radiation on fluid motion induced by a stretching sheet within a porous medium have been studied numerically. The radiative heat flux in the energy equation was modeled using the Rosseland diffusion approximation. Various physical influences, including heat generation and viscous dissipation, have been examined for their impact on heat-transfer characteristics. The governing system of partial differential equations was transformed into a system of dimensionless ordinary differential equations through appropriate similarity transformations. The HPM was then applied to obtain analytical solutions for these dimensionless equations. These dimensionless physical parameters have significant implications across numerous technical and environmental applications. Based on the numerical analysis conducted, the following conclusions can be drawn:

- The fluid temperature and velocity both improve with an increase in the radiation parameter R_d.
- The fluid velocity and temperature both decrease as the heat-source parameter R increases.
- The fluid velocity decreases with the magnetic parameter M but increases with the mixed convection parameter G_r.
- The temperature rises with an increase in the Eckert number E_c.
- Both the skin-friction coefficient and the heat-transfer rate decrease when the Prandtl number P_r increases.

Acknowledgments

None.

Funding

None.

Conflict of interest

The authors declare that they have no competing interests.

Author contributions

Conceptualization: All authors
Formal analysis: Gopinath Mandal
Investigation: All authors
Methodology: Babulal Talukdar
Writing–original draft: All authors
Writing–review & editing: All authors

Availability of data

The article contains the statistical data that underpin and validate the study's conclusions.

AI Tools Statement

Grammarly software is used for grammar refinement, and improving the clarity of the manuscript. No AI tools were used for data analysis, interpretation, or generating original scientific content.

References

1. Soundalgekar VM, Gupta SK, Birajdar NS. Effects of mass transfer and free convection currents on MHD Stokes' problem for a vertical plate. *Nucl Eng Des.* 1979;53(3):339–346. https://doi.org/10.1016/0029-5493(79)90060-8
2. Elbashbeshy EMA. Heat and mass transfer along a vertical plate with variable surface tension and concentration in the presence of the magnetic field. *Int J Eng Sci.* 1997;35(5):515–522. https://doi.org/10.1016/S0020-7225(96)00089-4
3. Sivaiah M, Nagarajan AS, Reddy PS. Heat and mass transfer effects on MHD free convective flow past a vertical porous plate. *IUP J Comput Math.* 2009;2(2):14–21. https://doi.org/10.1007/s10483-010-1355-6
4. Zueco J, Ahmed SS. Combined heat and mass transfer by mixed convection MHD flow along a porous plate with chemical reaction in presence of heat source. *Appl Math Mech.* 2010;31:1217–1230. https://doi.org/10.1007/s10483-010-1355-6
5. Hamza MM. Free convection slip flow of an exothermic fluid in a convectively heated vertical channel. *Ain Shams Eng J.* 2018;9(4):1313–1323. https://doi.org/10.1016/j.asej.2016.08.011
6. Hossain MA, Takhar HS. Radiation effect on mixed convection along a vertical plate with uniform surface temperature. *Heat Mass Transf.* 1996;31(4):243–248. https://doi.org/10.1007/BF02328616
7. AboEldahab EM. Radiation effect on heat transfer in an electrically conducting fluid at a stretching surface with a uniform free stream. *J Phys D Appl Phys.* 2000;33(24):3180. https://doi.org/10.1088/0022-3727/33/24/310
8. Muthucumaraswamy R, Senthil KG. Heat and mass transfer effects on moving vertical plate in the presence of thermal radiation. *Theor Appl Mech.* 2004;31(1):35–46. https://doi.org/10.2298/TAM0401035M
9. Kho YB, Hussanan A, Sarif NM, Ismail Z, Salleh MZ. Thermal radiation effects on MHD with flow heat and mass transfer in Casson nanofluid over a stretching sheet. *MATEC Web Conf.* 2018;150:06036. https://doi.org/10.1051/matecconf/201815006036
10. Kumar MA, Reddy YD, Rao VS, Goud BS. Thermal radiation impact on MHD heat transfer natural convective nanofluid flow over an impulsively started vertical plate. *Case Stud Therm Eng.* 2021;24:100826. https://doi.org/10.1016/j.csite.2020.100826
11. Sattar MA, Kalim H. Unsteady free-convection interaction with thermal radiation in a boundary layer flow past a vertical porous plate. *J Math Phys Sci.* 1996;30(1):25–37.
12. Cortell R. Effects of viscous dissipation and radiation on the thermal boundary layer over a nonlinearly stretching sheet. *Phys Lett A.* 2008;372(5):631–636. https://doi.org/10.1016/j.physleta.2007.08.005
13. Abel MS, Mahesha N. Heat transfer in MHD viscoelastic fluid flow over a stretching sheet with variable thermal conductivity, non-uniform heat source and radiation. *Appl Math Model.* 2008;32(10):1965–1983. https://doi.org/10.1016/j.apm.2007.06.038
14. Kim YJ. Unsteady MHD convective heat transfer past a semi-infinite vertical porous moving plate with variable suction. *Int J Eng Sci.* 2000;38(8):833–845. https://doi.org/10.1016/S0020-7225(99)00063-4
15. Asogwa KK, Ibe AA, Udo UM. Magnetohydrodynamic oscillatory viscoelastic flow with radiation and constant suction over a vertical flat plate in a porous medium. *IOSR J Math.* 2019;15(6):20–30. https://doi.org/10.9790/5728-1506052030
16. Pandey AK, Bhattacharyya K, Gautam AK, et al. Relationship between nonlinear mixed convection and thermal radiation. *Propuls Power Res.* 2023;12(1):153–165. https://doi.org/10.1016/j.jppr.2022.11.002
17. Mandal G. Convective-radiative heat transfer of micropolar nanofluid over a vertical non-linear stretching sheet. *J Nanofluids.* 2016;5(6):852–860. https://doi.org/10.1166/jon.2016.1265
18. Israel-Cookey C, Ogulu A, Omubo-Pepple VB. Influence of viscous dissipation and radiation on unsteady MHD free-convection flow past an infinite heated vertical plate in a porous medium. *Int J Heat Mass Transf.* 2003;46(13):2305–2311. https://doi.org/10.1016/S0017-9310(02)00544-6
19. Pal D, Mandal G, Vajravelu K. Mixed convective-radiative MHD heat and mass transfer of nanofluids over a stretching/shrinking sheet. *J Nanofluids.* 2016;5(3):340–350. https://doi.org/10.1166/jon.2016.1218
20. Abel MS, Sanjayanand E, Nandepanavar MM. Viscoelastic MHD flow and heat transfer over a stretching sheet with viscous and ohmic dissipations. *Commun Nonlinear Sci Numer Simul.* 2008;13(9):1808–1821. https://doi.org/10.1016/j.cnsns.2007.04.007
21. Sharma R, Bhargava R, Singh I. Combined effect of magnetic field and heat absorption on unsteady free convection in a micropolar fluid. *Appl Math Comput.* 2010;217(1):308–321. https://doi.org/10.1016/j.amc.2010.05.062
22. Mandal G. Magneto-radiative FeO–AlO–Cu/HO tri-hybrid nanofluid flow over a shrinking surface with entropy generation. *Int J Model Simul.* 2024:1-28. https://doi.org/10.1080/02286203.2024.2385115
23. He JH. Homotopy perturbation technique. *Comput Methods Appl Mech Eng.* 1999;178(3–4):257–262. https://doi.org/10.1016/S0045-7825(99)00018-3
24. He JH. Homotopy perturbation method: a new nonlinear analytical technique. *Appl Math Comput.* 2003;135(1):73–79. https://doi.org/10.1016/S0096-3003(01)00312-5
25. He JH. Homotopy perturbation method for bifurcation of nonlinear problems. *Int J Nonlinear Sci Numer Simul.* 2005;6(2):207–208. https://doi.org/10.1515/IJNSNS.2005.6.2.207
26. Beléndez A, Beléndez T, Márquez A, Neipp C. Application of He's homotopy perturbation method to conservative truly nonlinear oscillators. *Chaos Solitons Fractals.* 2008;37(3):770–780. https://doi.org/10.1016/j.chaos.2006.09.070

27. Ganji ZZ, Ganji DD. Approximate solutions of thermal boundary-layer problems by HPM. *Int J Nonlinear Sci Numer Simul.* 2008;9(4):415–422. https://doi.org/10.1515/IJNSNS.2008.9.4.415
28. Jhankal AK. Application of homotopy perturbation method for MHD free convection of water at 4°C. *Indian J Pure Appl Phys.* 2017;56:63–68.
29. Pal D, Mandal G, Vajravelu K. MHD convection–dissipation heat transfer over stretching and shrinking sheets. *Int J Heat Mass Transf.* 2013;65:481–490. https://doi.org/10.1016/j.ijheatmasstransfer.2013.06.017
30. Pal D, Mandal G. Mixed convection–radiation on stagnation-point flow with heat generation. *J Pet Sci Eng.* 2015;126:16–25. https://doi.org/10.1016/j.petrol.2014.12.006
31. Nia SH, Ranjbar AN, Ganji DD, Soltani H, Ghasemi J. Stability of nonlinear differential equations via HPM. *Phys Lett A.* 2008;372(16):2855–2861. https://doi.org/10.1016/j.physleta.2007.12.054
32. Wang CY. Free convection on a vertical stretching surface. *Z Angew Math Mech (ZAMM).* 1989;69(11):418–420. https://doi.org/10.1002/zamm.19890691115
33. Hussain ST, Nadeem S, Ul Haq R. Micropolar nanofluid flow over a stretching surface. *Eur Phys J Plus.* 2014;129(8):161. https://doi.org/10.1140/epjp/i2014-14161-8

Appendix

Additional information, data, and details of constants supporting the main finding.

$$a_1 = \frac{-\lambda + \sqrt{\lambda^2 + 4(M + 1/K)}}{2},$$

$$a_2 = \frac{-\lambda - \sqrt{\lambda^2 + 4(M + 1/K)}}{2},$$

$$d_1 = \frac{e^{10a_2}}{e^{10a_2} - e^{10a_1}},$$

$$d_2 = 1 - d_1,$$

$$a_3 = \frac{-P_r\lambda + \sqrt{P_r^2\lambda^2 + 4P_rR\left(1 + R_d\right)}}{2\left(1 + R_d\right)},$$

$$a_4 = \frac{-P_r\lambda - \sqrt{P_r^2\lambda^2 + 4P_rR\left(1 + R_d\right)}}{2\left(1 + R_d\right)},$$

$$d_3 = \frac{e^{10a_4}}{e^{10a_4} - e^{10a_3}}, d_4 = 1 - d_3,$$

$$d_7 = \frac{-G_r d_3^2}{4a_3^2 + 2\lambda a_3 - (M + 1/K)},$$

$$d_8 = \frac{-G_r d_4^2}{4a_4^2 + 2\lambda a_4 - (M + 1\backslash K)},$$

$$d_9 = \frac{-2G_r d_3 d_4}{\left(a_3 + a_4\right)^2 + \lambda\left(a_3 + a_4\right) - (M + 1/K)},$$

$$d_{10} = -\left(d_7 + d_8 + d_9\right),$$

$$d_{11} = -\left(d_7 e^{20a_3} + d_8 e^{20a_4} + d_9 e^{10(a_3 + a_4)}\right),$$

$$d_5 = \frac{d_{11} - d_{10}e^{10a_2}}{e^{10a_1} - e^{10a_2}},$$

$$d_6 = d_{10} - d_5,$$

$$d_{14} = \frac{-P_r E_c a_1^2 d_1^2}{4a_1^2\left(1 + R_d\right) + 2P_r\lambda a_1 - P_r R},$$

$$d_{15} = \frac{-P_r E_c a_2^2 d_2^2}{4a_2^2\left(1 + R_d\right) + 2P_r\lambda a_2 - P_r R},$$

$$d_{16} = \frac{-P_r E_c a_1 d_1 a_2 d_2}{\left(1 + R_d\right)\left(a_1 + a_2\right)^2 + P_r\lambda\left(a_1 + a_2\right) - P_r R},$$

$$d_{17} = -\left(d_{14} + d_{15} + d_{16}\right),$$

$$d_{18} = -\left(d_{14} e^{20a_1} + d_{15} e^{20a_2} + d_{16} e^{10(a_1 + a_2)}\right),$$

$$d_{12} = \frac{d_{18} - d_{17}e^{10a_4}}{e^{10a_3} - e^{10a_4}},$$

$$d_{13} = d_{17} - d_{12}$$